Int. Journ. of Peening Science and Technology, Vol. 1, pp. 99–118
Reprints available directly from the publisher
Photocopying permitted by license only.

Finite Element Analysis of Residual Stress Induced by Multiple Laser Shock Peening with Square Spots

R. ZHU[1], Y.K. ZHANG[2], G.F. SUN[1], S.B. ZHANG[1], P. LI[1] AND Z.H. NI[1]

[1]*Jiangsu Key Lab Design &MfgMicronano Biomed Ins, Southeast University, Nanjing, Jiangsu 211189, China*
[2]*School of Electromechanical Engineering, Guangdong University of Technology, Guangzhou, Guangdong 510006, China*

Laser shock peening (LSP) is a competitive innovative surface treatment technique, which can induce compressive residual stresses in metal materials. In this investigation, a modified explicit finite element analysis (FEA) method was used to predict the residual stress distribution in 2050-T8 aluminum alloy induced by LSP. The laser shock sequence was programmed by VDLOAD ABAQUS subroutine. Simulated residual stresses from FEA showed good consistency with open literatures. Based on the method, the effects of LSP parameters such as overlapping percentage, number of impacts, laser power density, laser spot size on the average surface residual stress and average in-depth residual stress of 2050-T8 aluminum alloy were analyzed.

Keywords: *Laser shock peening, residual stress, modified explicit simulation*

1 INTRODUCTION

Over the past decades, laser shock peening (LSP) has been proposed as a competitive surface treatment technique [1], which can generate deeper compressive residual stress compared to those characteristics of the conventional shot peening, improve fatigue life [2], stress corrosion [3] and wear resistance [4] of metallic materials.

*Corresponding author's e-mail: gfsun@seu.edu.cn

With the development of laser technology, square shaped laser spot has been used in LSP. It has shown more efficient coverage, overlapping, uniform packing and improved surface quality for a layer of treatment as compared to the round shaped spot [1]. In order to predict the residual stress field and optimize LSP parameters, many experiments and analytical models have been reported in the literatures [5-10]. In the meantime, a number of finite element models (FEM) have been applied to simulate the confined LSP process. The conventional method involves two distinct steps using both explicit and implicit solving techniques to obtain an absolutely steady residual stress field. Braisted and Brockman [11] first adopted the combined approach to predict the residual stress distribution induced by LSP technologies in Ti-6Al-4V and 35CD4 steel in 1999. From then on, several researchers have used this method to analyse the laser shock waves propagated into different metallic materials, and predict residual stress distribution and surface deformation of the metal targets [12-17]. However, when there are multiple laser shocks, the above-mentioned method becomes difficult to be carried out. In order to meet the requirements of practical industrial applications, a variety of LSP parameters need to be considered for multiple laser shocks.

In view of the above-mentioned facts, this investigation adopted a modified explicit procedure [18] to predict the distribution of residual stress induced by LSP. Basic simulation for the LSP treatment of 25 impact loadings was calculated and validated. In addition, the influences of different LSP parameters such as overlapping percentage, number of impacts, laser power density, laser spot size were investigated.

2 3-D FEM AND VALIDATION

2.1 LSP analysis procedure

The modified explicit simulation approach adopted for LSP contains two analysis steps [18]. The first is used for each LSP with a short duration explicit approach until the kinetic energy approximates zero. The second is used for the final shot with an extended-duration explicit approach instead of implicit analysis. The modified explicit simulation approach should adopt infinite elements as non-reflecting boundaries and it is based on the observation that the redistribution of residual stress field drops when a transient stress state is steady. For a multi-shot simulation, the pulse shock sequence was implemented into ABAQUS/Explicit by using VDLOAD subroutine. The procedure of LSP simulation is shown in Figure 1.

2.2 High pressure pulse for LSP process

During an LSP process, a high intensity laser pulse vaporizes an absorbent layer, forming plasma and producing an extremely high pressure on the material surface with a short duration pulse pressure. The expression for the peak pressure P is given by Fabbro et al. [19]:

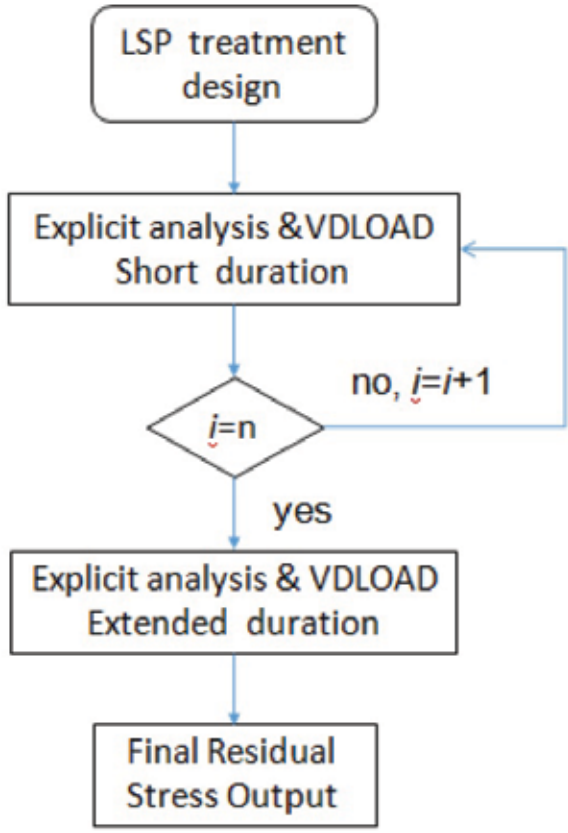

FIGURE 1
Laser Shock Peening Simulation Procedure.

$$P(\text{kbars}) = 0.10\left(\frac{\alpha}{2\alpha+3}\right)^{1/2} Z^{1/2}\left(g/cm^2 s\right) I_0^{1/2}\left(GW/cm^2\right) \qquad (1)$$

where α is the efficiency of the internal energy devoted to the thermal energy, I_0 is the absorbed laser power density, Z is the reduced acoustic impedance between the target Z_{target} and the confining medium water Z_{water}.The model considers the plasma to be a perfect gas and the impedance between two materials is defined by the relation:

$$\frac{2}{Z} = \frac{1}{Z_{water}} + \frac{1}{Z_{target}} \qquad (2)$$

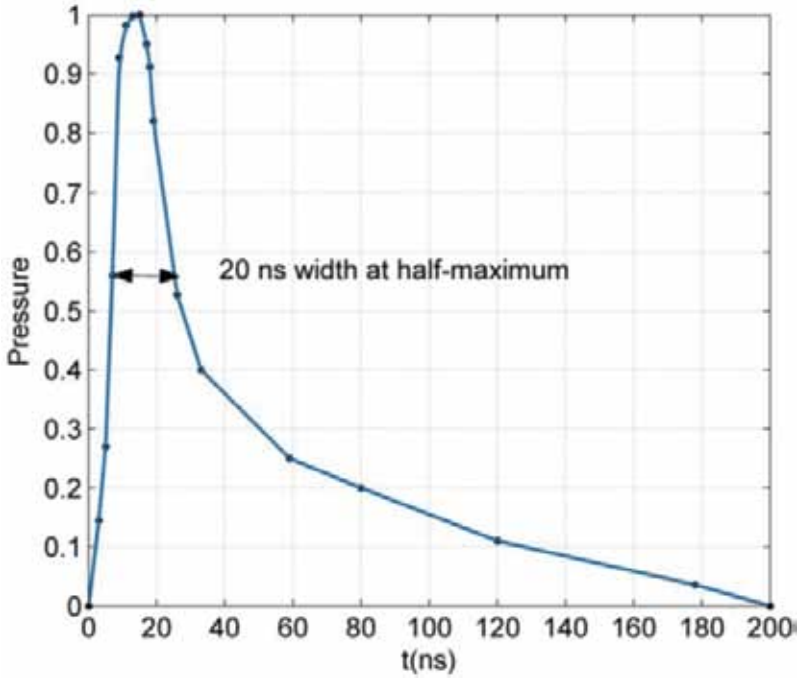

FIGURE 2
Normalized pressure pulse induced by a 8-10ns laser pulse used in ABAQUS.

For the aluminum target, we take $Z_{target} = 1.5 \times 10^6$ g/cm^2 s and $Z_{water} = 0.165 \times 10^6$ g/cm^2 s in the calculation, The value of α varies in a range of 0.2 to 0.5, and it just depends on the transparent confining layer and the other processing conditions [20]. α =0.35 is used and the peak pressure is given in Equation (3):

$$P(Gpa) = 1.65\sqrt{I_0(GW/cm^2)} \tag{3}$$

Owing to the fact that square spot shows better homogenous in intensity, the spatial distribution of shock pressure is presumed to be uniform. The typical profile of pressure pulse history evolution obtained from experiments is given in Figure 2 [21].

In the work, we imposed a fixed number of pressure pulse impacting a target material successively as shown in Figure 3. The averaged residual stresses $\sigma_{xx} = \sigma_{11}$ at the surface and along the depth of the target were considered. In addition, the overlapping percentage $R\%$ was defined by $R\% = \Delta d/d$ with d = laser spot size and Δd =distance between two adjacent laser impacts.

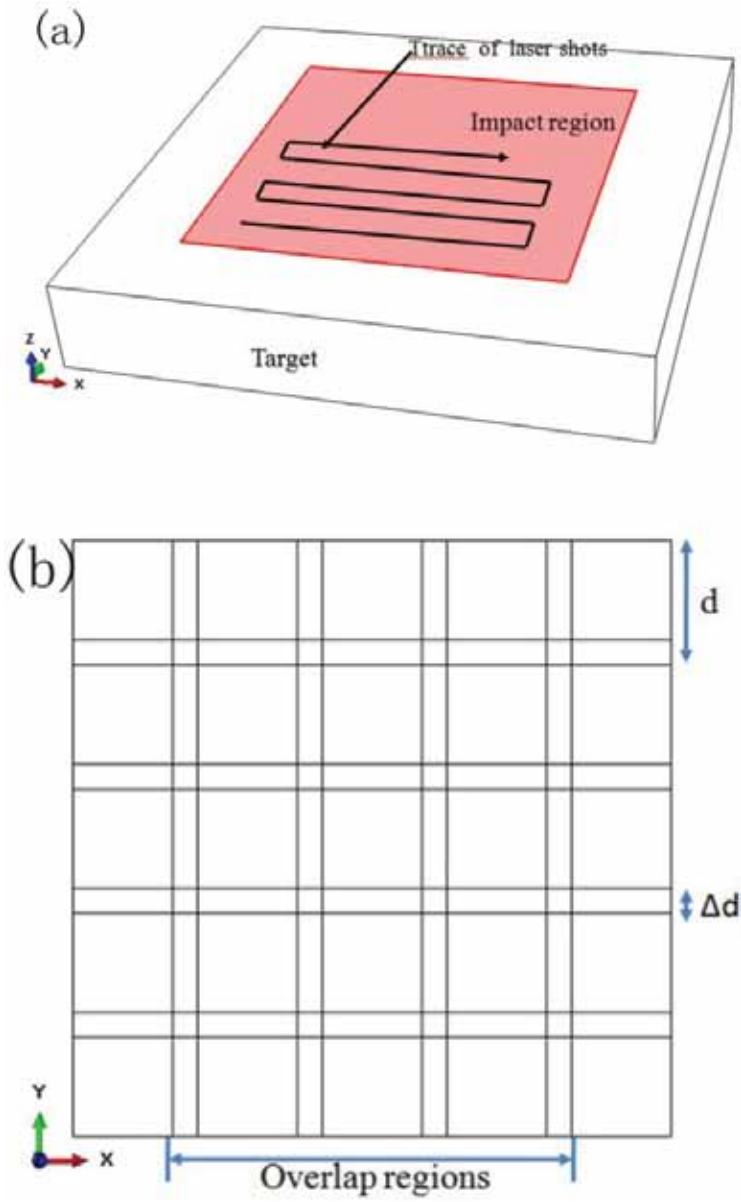

FIGURE 3
(A) The geometry of LSP, (b) schematic illustration of overlapped LSP.

2.3 Constitutive model and material properties

In LSP processes, the strain rate is in the order of 10^6/s. In order to accurately predict the material response, the Johnson-Cook model was adopted as the constitutive model to deal with high strain rate problems. Due to the fact that

TABLE 1
Mechanical properties of 2050-t8 aluminum alloy[21].

Material	*A* (MPa)	*B* (MPa)	*n*	*C*	ε_0 (/s)	*E* (Gpa)	υ	ρ kg/m^3
2050-T8	510	200	0.45	0.02	0.01	72	0.33	2750

thermal effect in LSP process is minimal, the thermal part of Johnson-cook model could be removed in the finite element simulations. Therefore, the equivalent Von Mises flow stress is given by:

$$\sigma = \left(A + B\varepsilon^n\right)\left[1 + CLn\left(\frac{\dot{\varepsilon}}{\dot{\varepsilon}_0}\right)\right] \tag{4}$$

where ε is the equivalent plastic strain, $\dot{\varepsilon}$ represents dynamic strain rate, and $\dot{\varepsilon}_0$ is the quasi-static strain rate, *A, B, C* and *n* are considered to be the material constants (*A* is the yield stress at 0.2% offset strain, *B* is the work hardening modulus, *n* represents the work hardening exponent and *C* represents the strain rate sensitivity). 2050-T8 aluminum alloy is the material considered for this investigation. The material property parameters required for FEM simulation are illustrated in Table 1.

2.4 Modeling of the LSP process

A three-dimensional (3D) dynamic FEM was developed to simulate the process of 25 square laser spots impacting on the target surface. Corresponding 3D model is shown in Figure 4(a). For the element type, two types of elements (C3D8R for finite elements and CIN3D8 for infinite elements) are used, as shown in Figure 4(b). The infinite elements are used as non-reflecting boundaries, which will prevent shock wave reflections on free surfaces from backing into the finite element area and also can reduce the computational time. Up to 2532495 continuums three dimensional eight-node with reduced integration elements were used to mesh the FEM. An element size of 150μm×150μm×100μm was used within the shocked region.

2.5 Modified method validation

The modified method is validated by comparing computed results with available experimental data and FEA results from Hfaiedh et al [21], in which a specimen of 2050-T8 aluminum alloy with a size of 25mm×25mm×5mm was treated by 25 laser impacts. In the literature, the spot size of 1.5mm, the overlap of 50%, the laser power density of 3.5 GW/cm^2 , and laser pulse of 10ns were used in the LSP process. Figure 5 shows the kinetic energy history from the LSP simulation. It can be seen that kinetic energy approaches zero for

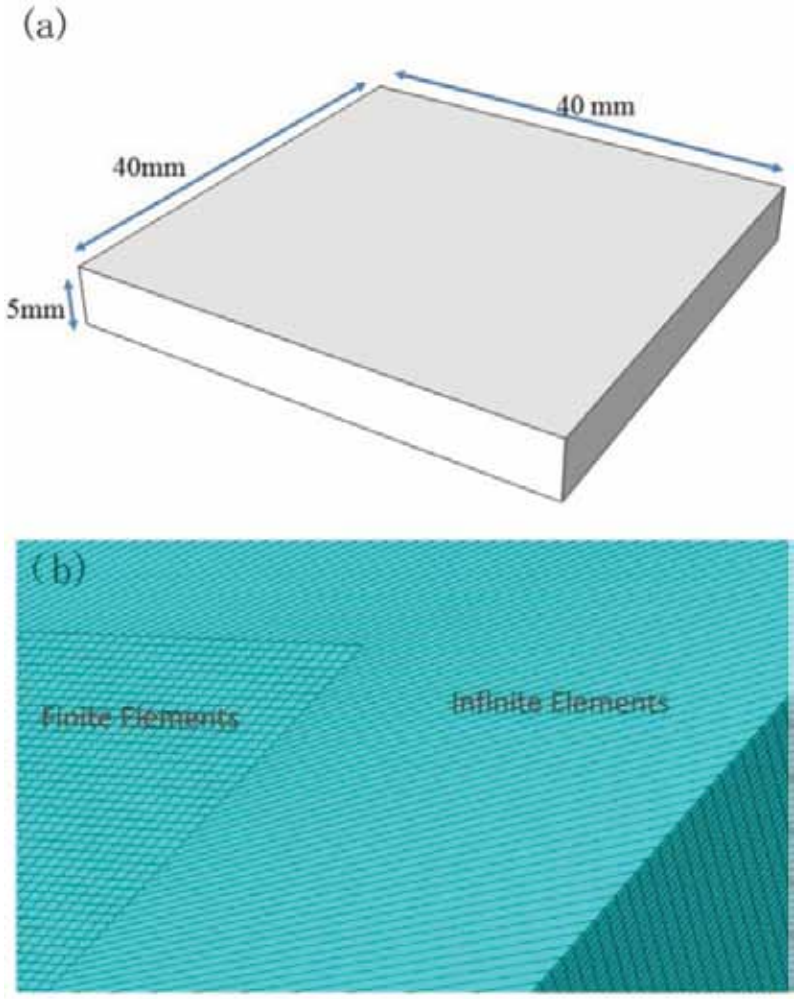

FIGURE 4
(A) 40mm×40mm×5mm 3-D model, (B) 3d fem mesh.

each LSP shot when the short duration reaches 8×10^{-6}s. Therefore, 8×10^{-6}s can be selected as the short duration and 4×10^{-5}s is selected as extended duration.

The comparison of surface residual stress σ_{11} is shown in Figure 6. It shows the simulated values (in grey lines in Figure 6a and b) from different data extraction lines and average simulated values (black line in Figure 6a and b). Similarly, the comparison of in-depth residual stress σ_{11} (Figure 7) also corresponds to average simulated values. The comparison shows a good similarity between simulations and the data from literature. Therefore, it

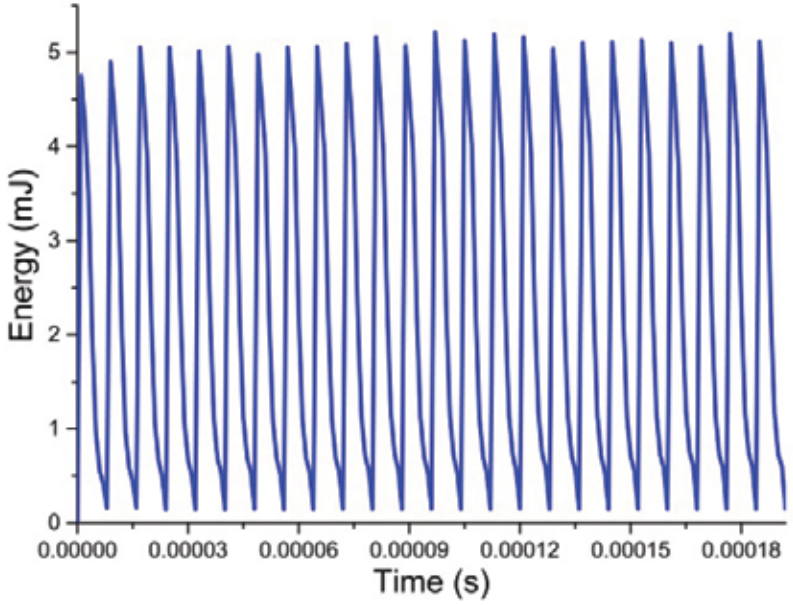

FIGURE 5
Kinetic energy history in each short duration.

could be concluded that the modified calculation method is reliable to simulate residual stress and can be used further to predict residual stress distribution in the target induced by LSP.

3 RESULTS AND DISCUSSION

3.1 Influence of overlapping percentage

Figure 8 shows the residual stress distributions of 25 impacts on 2050-T8 aluminum alloy when laser power density is 3.5GW/cm^2 , laser spot size is 3 mm, laser pulse is 10 ns, and overlapping rate is 5%. The average simulated values of residual stresses σ_{11} at the surface and along the depth of the target were considered using the inserted black dot lines (Figure 8 a and 8b).

Overlapping percentage can drastically affect the surface residual stress distribution and depth of residual stress during massive LSP impacts. 5% and 50% overlapping rates were applied to investigate the influence and other parameters used in the simulations were: laser power density of 3.5 GW/cm^2 , laser spot size of 3mm and laser pulse duration of 10ns.

Figure 9(a) shows that the surface residual stress across overlap regions tends to increase with overlapping percentage. The surface residual stress

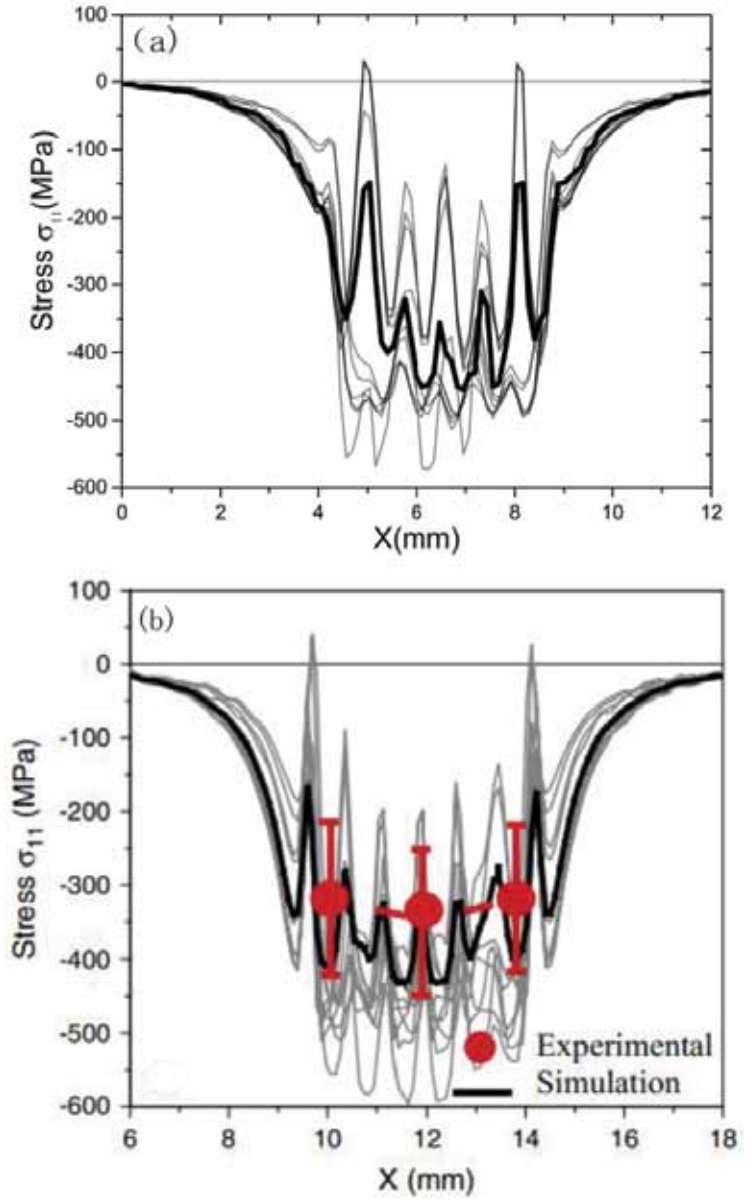

FIGURE 6
Comparison of surface residual stress σ_{11}, (a) modified calculation method, (b) reference values [21].

distributions of 50% overlap are more uniform than those of 5% overlap in the overlap regions. The non-uniformity of the residual stress field caused by the focusing of the radial stress waves has been considered, which can be defined by the following equation:

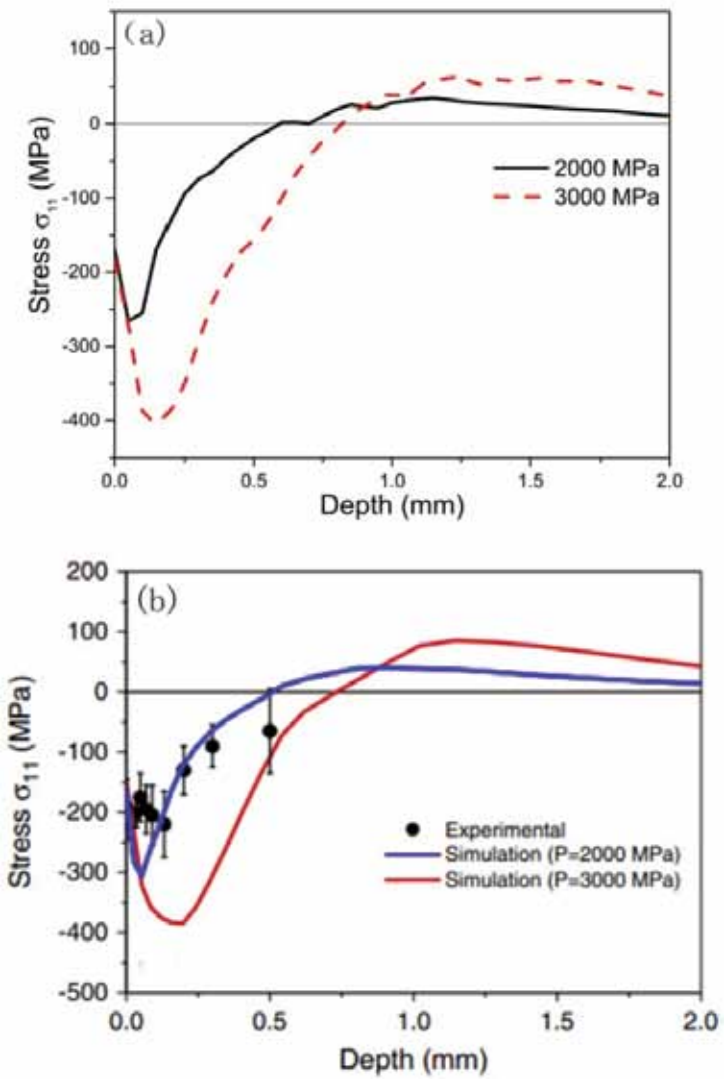

FIGURE 7
Comparison of in-depth residual stress , (a) modified calculation method, (b) reference values [21].

$$\phi = \frac{\sigma_{11}^{\max} - \sigma_{11}^{center}}{\sigma_{11}^{\max}} \times 100\% \tag{5}$$

where ϕ is the fluctuation ratio, σ_{11}^{max} is the maximum surface residual stress and σ_{11}^{center} is the surface residual stress of the spot center in the overlap regions. Table 2 shows the results of surface residual stress with different overlapping percentages obtained by numerical simulations.

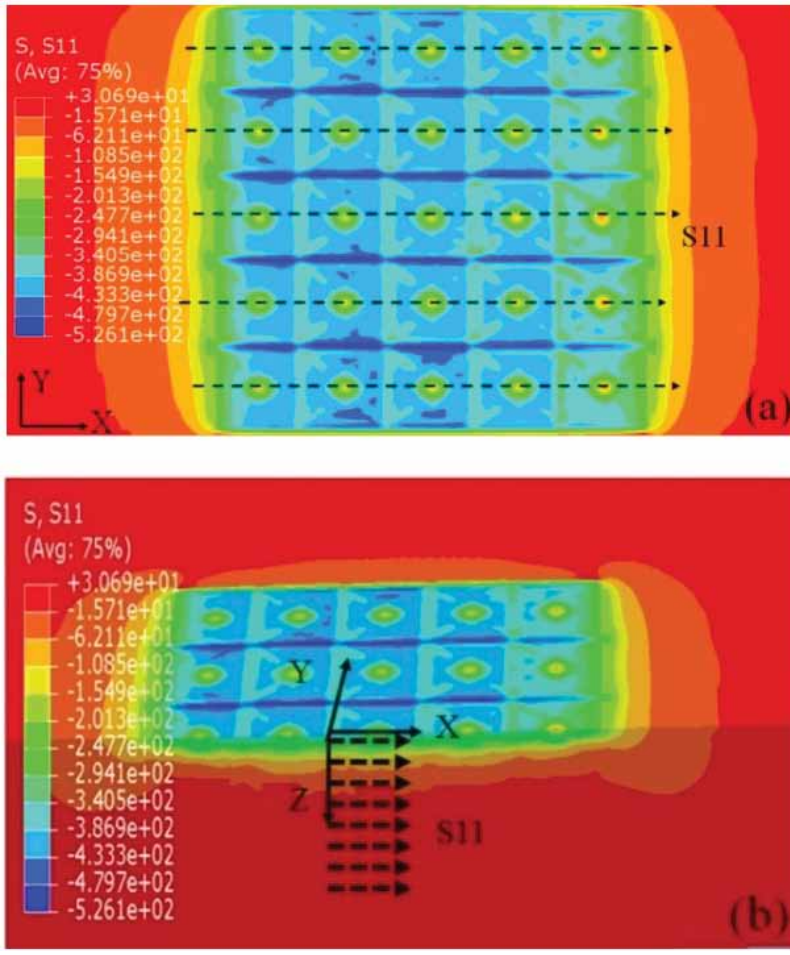

FIGURE 8
Residual stress distributions of simulated data, (a) surface residual stress, (b) in-depth residual stress.

Figure 9(b) exhibits the simulated in-depth residual stress. It indicates that the in-depth residual stress and plastically affected depth increase with the increase of overlapping percentage. The reason is that the overlap regions with an overlapping percentage of 50% suffer repeated LSP impacts. It can be seen that the number of LSP impacts reaches four across the overlap regions with 50% overlap. The residual stress and plastically affected depth generally increase with the increasing LSP impacts in a certain range.

3.2 Influence of multiple impacts

The surface and in-depth residual stress distributions that result from different numbers of impacts are shown in Figure 10. The LSP parame-

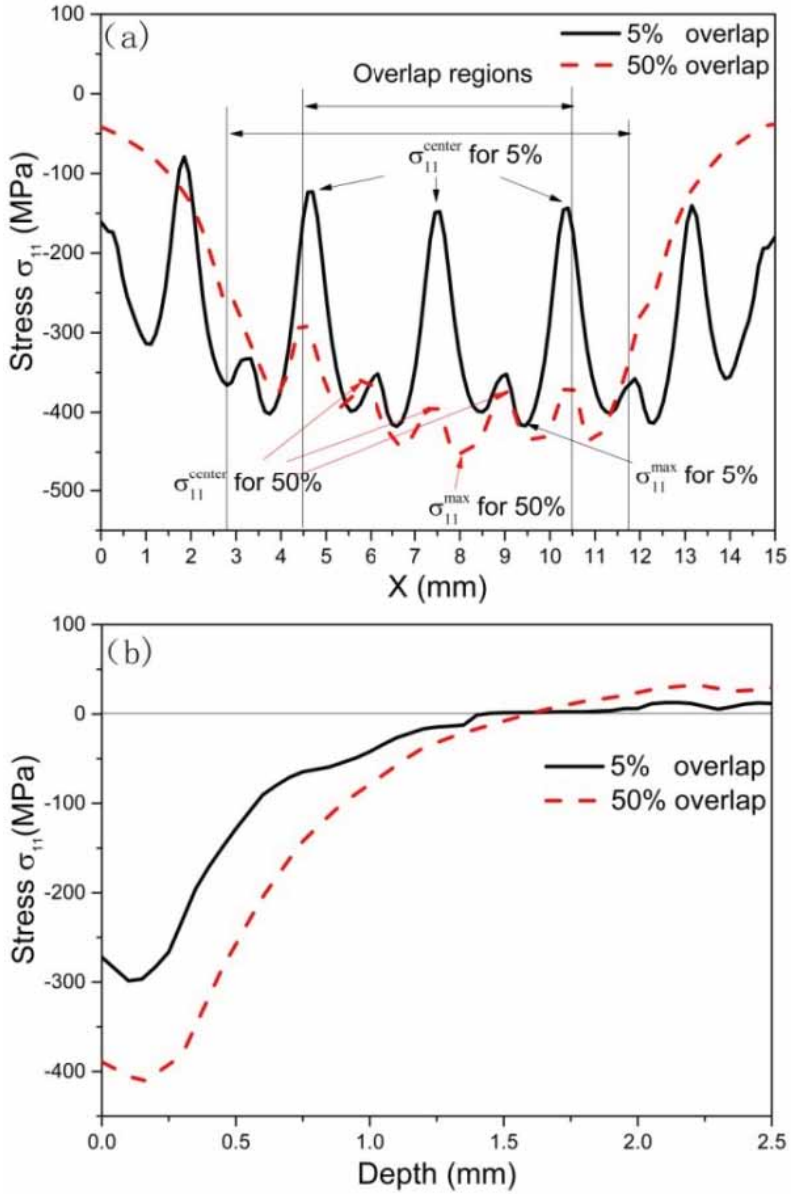

FIGURE 9
Influence of overlapping percentage on residual stress distribution, (a) surface residual stress, (b) through-thickness residual stress.

ters such as laser power density, laser spot size, laser pulse duration, and overlapping percentage used in the simulations were defined to be 3.5 GW/cm^2, 5mm, 10ns, and 50%, respectively. Fig. 11 shows a schematic

TABLE 2
Results of surface residual stress with different overlapping rates in the overlap regions.

Overlapping rate		(x, σ_{11}^{max} (mm, MPa)	(x, σ_{11}^{center} (mm, MPa)	ϕ
1.	5%	(9.45, -416.8)	(4.65,-123.1)	70.4%
2.	5%	(9.45, -416.8)	(7.5, -147.8)	64.5%
3.	5%	(9.45, -416.8)	(10.35,-143.5)	65.6%
4.	50%	(7.86, -450.5)	(6, -355.1)	21.2%
5.	50%	(7.86, -450.5)	(7.5, -391.3)	13.1%
6.	50%	(7.86,-450.5)	(9, -372.3)	17.3%

of 25 overlapped LSP shots for 50% overlap. As shown in Fig. 11, 1, 2, 3 and 4 represent four square spots. A represents the overlapped region of four square spots. When the overlapping percentage is 50%, the overlapped region suffers four impacts on the trace of laser shock for the first impact and twelve impacts on the trace of laser shock after the third impact. This explains why the stress after 3 impacts was lower than 1 impact in the overlapped area.

As shown in Figure 10(a), the surface residual stress of overlap regions decreases slightly with the increase of number of impacts on the same location. This result can be attributed to that surface deformations increase with the increasing number of impacts and it will induce the stress relaxation in the heavily deformed region. Literature [22] gave the similar results. Figure 10(b) shows that in-depth residual stress increases with increasing number of impacts, which is already evidenced analytically by Wei et al [12]. Hence, multiple impacts can have a beneficial effect on in-depth residual stress distributions.

3.3 Influence of laser power density

The peak pressure as a function of laser power density has been defined in Equation (3). It will create plastic strain when the peak pressure exceeds the shock yield strength(or Hugoniot limit *HEL*) ,which can be defined according to [21]:

$$P_H = \frac{1}{2}\rho \times C_{el} \times U_F \tag{6}$$

With C_{el}=elastic wave velocity=6000m/s, ρ=2750kg/m^3, U_F=free surface velocity=170m/s, we obtain Hugoniot limit value P_H=1.4 GPa.

The power density used for the simulation was assumed 1.5 GW/cm^2, 2.5 GW/cm^2, 3.5 GW/cm^2, and 4.5 GW/cm^2, corresponding to estimated peak pressures 2GPa, 2.6GPa, 3GPa, and 3.5GPa using Equation (3). In

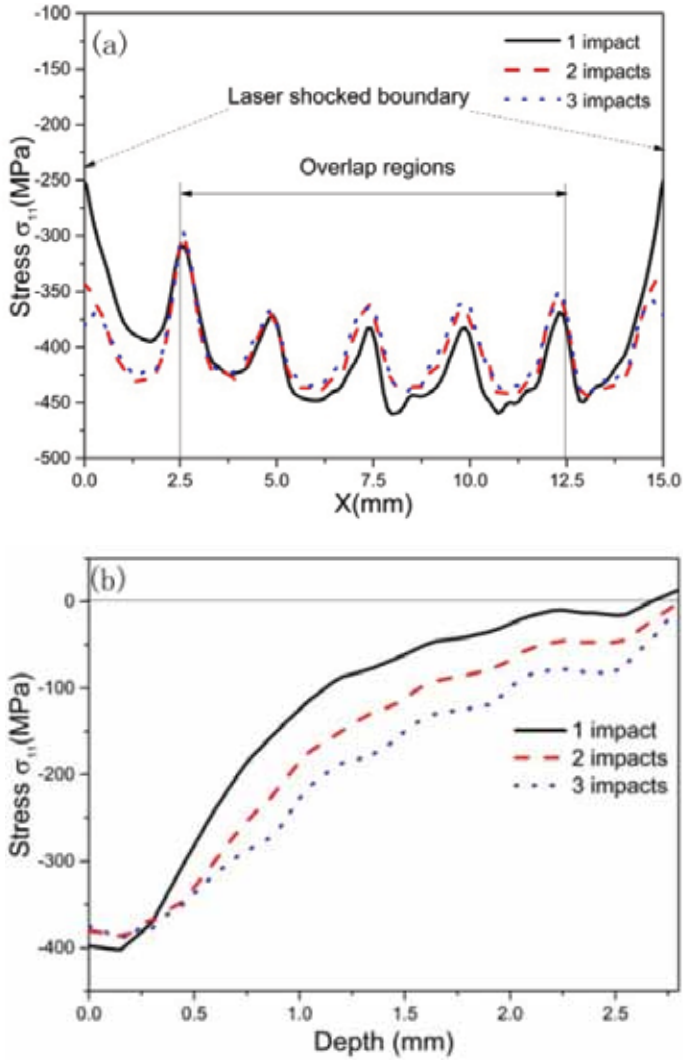

FIGURE 10
Influence of number of impacts on residual stress distribution, (a) surface residual stress, (b) in-depth residual stress.

addition, the simulation for each case was accomplished using the same LSP parameters (5mm spot size,10ns laser pulse duration and 50% overlap).

Figure 12(a) shows that surface residual stress increases with increasing power densities. The variation becomes small when laser power density

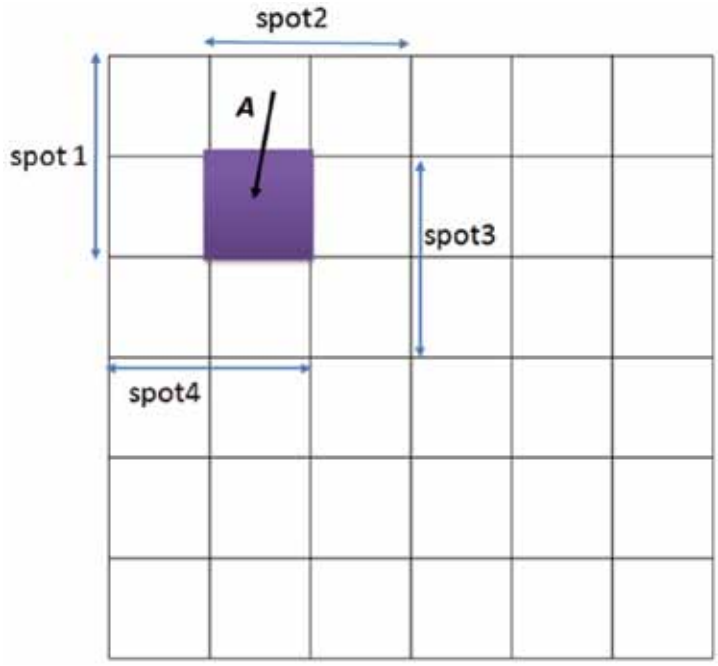

FIGURE 11
Schematic of overlapped 25 LSP shots for 50% overlap.

increases to 3.5 GW/cm^2. When the laser power density is in the range of 2.8 to 4.5 GW/cm^2 , corresponding peak pressure is between 2.8GPa and 3.5GPa, which is within the (2 to 2.5) × P_H range. The phenomenon is consistent with literature [23], which indicates that P= (2 to 2.5) × P_H is the optimum pressure for treatment of materials.

Figure 12(b) shows the residual stress along the depth of the target. As reported by Peyre [23] more than 20 years ago, the plastically affected depth increases with increasing power densities. Therefore, laser power density is a very important parameter to be optimized for generating residual stress fields.

3.4 Influence of laser spot size

In order to analyze the influence of spot size on residual stress distribution, the spot size was assumed to be 3mm, 4mm, and 5mm. The 3.5 GW/cm^2 laser power density , 10ns laser pulse duration, and 50% overlap were kept consistent in the simulations.

The results in Figure 13(a) show that surface residual stress distributions of overlap regions are quite similar to the variation of the laser spot size. However, the surface residual stress of laser shocked boundary

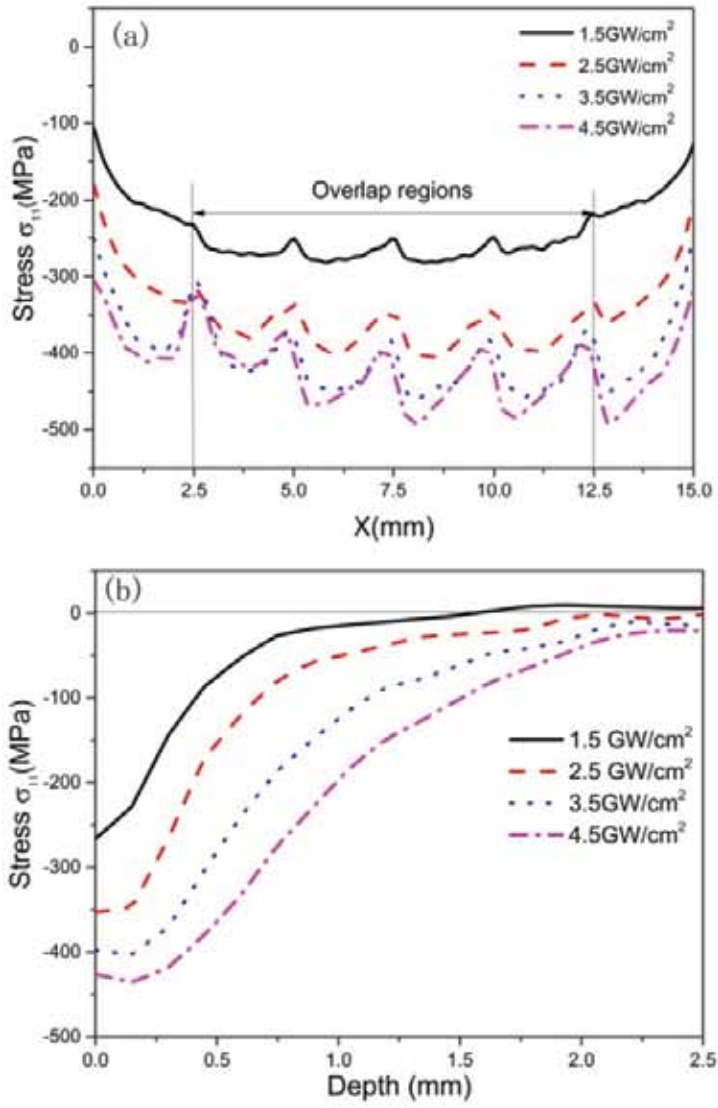

FIGURE 12
Influence of laser power density on residual stress distribution, (a)surface residual stress, (b) in-depth residual stress.

increases with increasing spot size. Increasing the laser spot size can also increase the depth of the residual stress. Figure 13(b) shows the distribution of in-depth residual stresses for d=3mm, 4mm and 5mm, respectively. It can be seen that plastically affected depth is increased by 36% as a result of increasing the laser spot size from 3 mm to 5 mm, which is evidenced by Peyre et al [24].

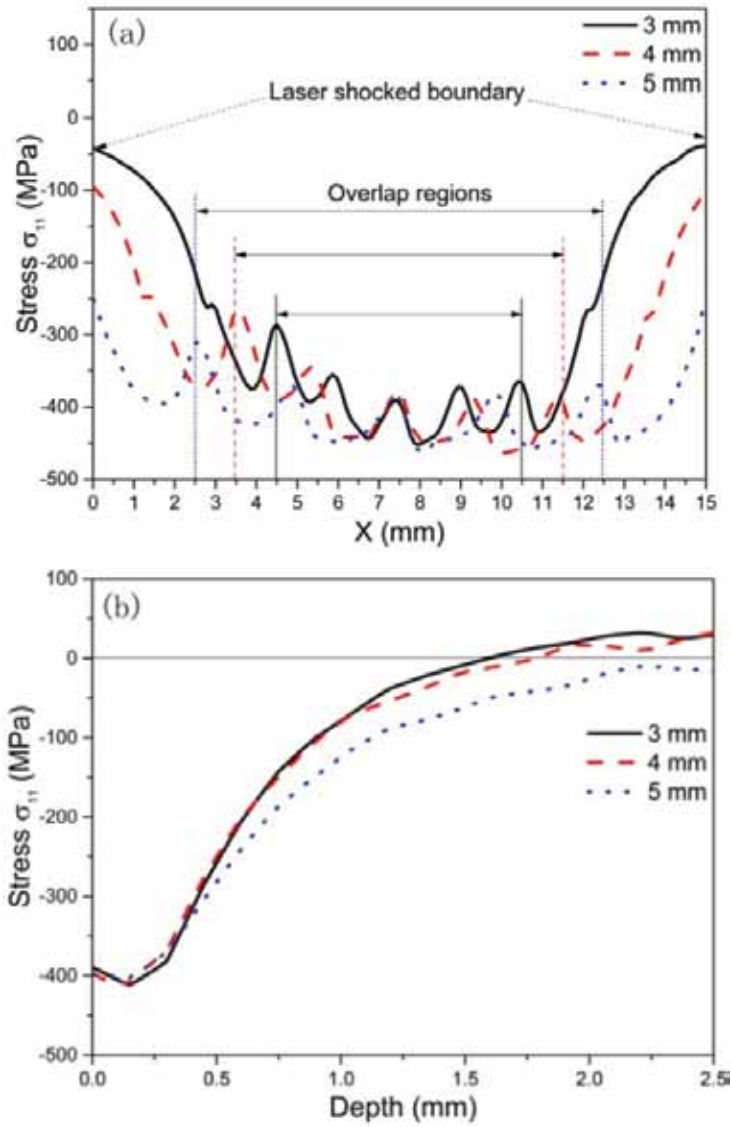

FIGURE 13
Influence of laser spot size on residual stress distribution, (a)surface residual stress, (b) through-thickness residual stress.

4 CONCLUSIONS

A three-dimensional model was proposed to predict the distribution of the average residual stresses field of 2050-T8 aluminum alloy after LSP treatment with multiple square spots. The following conclusions can be made.

(i) The modified explicit simulation was performed and verified with available results from literature. The use of VDLOAD subroutine makes the multi-spots three dimensional LSP simulation more convenient.
(ii) Compared with 5% overlap, 50% overlap can generate larger residual stresses with good uniformity and deeper plastically affected depth.
(iii) The surface residual stresses decrease with the increase of number of impacts for overlap regions, while the in-depth residual stresses increase with increasing the number of impacts.
(iv) P= (2 to 2.5) × P_H is the optimum pressure for LSP in this investigation. It can generate larger surface residual stresses and deeper plastically effected depth.
(v) The plastically effected depth increases with increasing the spot size, which implies that a larger spot size tends to produce a larger plastically affected depth of compressive residual stresses.

ACKOWLEDGEMENTS

This work was supported by the Joint Fund of Advanced Research of Equipment and Ministry of Education of China (Grant number 6141A02033103); the Scientific and Technological Innovation Project of Certain Commission of China (grant number 1716313ZT01001801); the Industry-University-Institute Cooperation Joint Research Project of Jiangsu Province of China (grant number BY2015070-05); the Six Talent Peaks of Jiangsu Province (grant number 2016-HKHT-001); the China Postdoctoral Science Foundation (grant numbers 2015M570395, 2016T90400); and the Postdoctoral Science Foundation of Jiangsu Province (grant number 1501028A).

NOMENCLATURE

A	Yield stress at 0.2% offset strain(MPa)
B	Work hardening modulus(MPa)
C	Strain rate sensitivity
n	Work hardening exponent
P	Peak pressure induced by laser beam(GPa)
Z	Reduced acoustic impedance(g/cm^{2}s)
Z_{target}	Shock impedance of the 2050-T8 aluminum alloy(g/cm^{2}s)
Z_{water}	Shock impedance of the water(g/cm^{2}s)
E	Elastic modulus(GPa)
I_0	Absorbed laser power density (GW/cm^2)

R%	Overlapping percentage
d	Laser spot size(mm)
Δd	Distance between two adjacent laser impacts(mm)
ϕ	Fluctuation ratio
C_{el}	Elastic wave velocity(m/s)
U_F	Free surface velocity (m/s)
P_H	Hugoniot limit value(GPa)

Greek symbols

σ_{11}^{max}	Maximum surface residual stress in the overlap regions(MPa)
σ_{11}^{center}	Surface residual stress of the spot center in the overlap regions(MPa)
ρ	Density of the 2050-T8 aluminum alloy(kg/m^3)
σ	Equivalent Von Mises flow stress(MPa)
v	Poisson's ratio
ε	Equivalent plastic strain
$\dot{\varepsilon}$	Dynamic strain rate
$\dot{\varepsilon}_0$	Quasi-static strain rate
α	Efficiency of the internal energy devoted to the thermal energy

REFERENCES

[1] Gujba, A. K, and Medraj, M. Laser peening process and its impact on materials properties in comparison with shot peening and ultrasonic impact peening. *Materials* **7** (2014), 7925-7974.

[2] Montross, C. S., Wei, T., Ye, L., Clark, G. and Mai, Y.W. Laser shock processing and its effects on microstructure and properties of metal alloys: A review. *International Journal of Fatigue* **24** (2002), 1021-1036.

[3] Hua, Y.Q., Bai, Y.C., Ye, Y.X., Xue, Q., Liu, H.X., Chen, R.F. and Chen, K.M. Hot corrosion behavior of TC11 titanium alloy treated by laser shock processing. *Applied Surface Science* **283** (2013), 775-780.

[4] Lim, H., Kim, P., Jeong, H. and Jeong, S. Enhancement of abrasion and corrosion resistance of duplex stainless steel by laser shock peening. *Journal of Materials Processing Technology* **212** (2012),1347-1354.

[5] Dorman, M., Toparli M.B., Smyth, N., Cini, A., Fitzpatrick, M.E. and Irving, P.E. Effect of laser shock peening on residual stress and fatigue life of clad 2024 aluminium sheet containing scribe defects. *Materials Science and Engineering: A* **548** (2012), 142-151.

[6] Gagliardi, M.A., Sencer, B.H., Hunt, A.W., Maloy, S.A. and Gray, G.T. Relative defect density measurements of laser shock peened 316L stainless steel using positron annihilation spectroscopy. *Journal of Nondestructive Evaluation* **30** (2011), 221-224.

[7] Qiao, H.C., Zhao, J.Z. and Gao, Y. Experimental investigation of laser peening on TiAl alloy microstructure and properties. *Chinese Journal of Aeronautics* **28** (2015), 609-616.

[8] Cao, Z.W., Xu, H., Zou, S.K. and Che, Z.G. Investigation of surface integrity on TC17 titanium alloy treated by square-spot laser shock peening. *Chinese Journal of Aeronautics* **25** (2012), 650-656.

[9] Lou, S., Li Y., Zhou L., Nie, X., He, G., Li, Y. and He, W. Surface nanocrystallization of metallic alloys with different stacking fault energy induced by laser shock processing. *Materials & Design* **104** (2016), 320-326.

[10] Yu, Q., Dong Z., Miao R., Deng, X. and Chen, L. Bending deformation of laser peened aluminium alloy with uniform rectangular spots. *Materials Science and Technology* **32** (2016), 9-14.

[11] Braisted, W. and Brockman, R. Finite element simulation of laser shock peening. *International Journal of Fatigue* **21** (1999), 719-724.

[12] Wei, X.L. and Ling, X. Numerical modeling of residual stress induced by laser shock processing. *Applied Surface Science* **301** (2014), 557-563.

[13] Cao, Z.W., Che, Z.G., Zou, S.K. and Fei, Q.X. Numerical simulation of residual stress field induced by laser shock processing with square spot. *Journal of Shanghai University* **15** (2011), 553-556.

[14] Hu, Y.X., Gong, C.M., Yao, Z.Q. and Hu, J. Investigation on the non-homogeneity of residual stress field induced by laser shock peening. *Surface & Coatings Technology* **203** (2009), 3503-3508.

[15] Hu, Y.X., Yao, Z.Q., Wang, F. and Hu, J. Study on residual stress of laser shock processing based on numerical simulation and orthogonal experimental design. *Surface Engineering* **23** (2007), 470-478.

[16] Ding, K. Three-dimensional dynamic finite element analysis of multiple laser shock peening processes. *Surface Engineering* **19** (2003), 351-358.

[17] Kim, J.H., Kim, Y.J., Lee, J.W. and Yoo, S.H. Study on effect of time parameters of laser shock peening on residual stresses using FE simulation. *Journal of Mechanical Science and Technology* **28** (2014), 1803-1810.

[18] Vasu, A., Hu Y. and Grandhi, R.V. Differences in plasticity due to curvature in laser peened components. *Surface & Coatings Technology* **235** (2013), 648-656.

[19] Fabbro, R., Fournier J., Ballard P., Devaux, D. and Virmont, J. Physical study of laser produced plasma in confined geometry. *Journal of Applied Physics* **68** (1990), 775-784.

[20] Clauer, A. H. and Lahrman, D. F. Laser shock processing as a surface enhancement process. *Key Engineering Materials* **197** (2001), 121-144.

[21] Hfaiedh, N., Peyre P., Song H., Popa, I., Ji V. and Vignal, V. Finite element analysis of laser shock peening of 2050-T8 aluminum alloy. *International Journal of Fatigue* **70** (2015), 480-489.

[22] Zhu, R.H., Xie H.M., Xue Y.F., Wang, L. and Li Y.J. Fabrication of speckle patterns by focused ion beam deposition and its application to micro-scale residual stress measurement. *Measurement Science and Technology* **26** (2015),095601.

[23] Peyre, P. and Fabbro, R. Laser shock processing: a review of the physics and applications. *Optical and Quantum Electronics* **27** (1995),1213-1229.

[24] Peyre, P., Berthe L., Scherpereel, X. and Fabbro R. Laser-shock processing of aluminium-coated 55C1 steel in water-confinement regime, characterization and application to high-cycle fatigue behaviour. *Journal of Materials Science* **33** (1998), 1421-1429.